Available online at www.sciencedirect.com

ScienceDirect

Journal of Ocean Engineering and Science 1 (2016) 325–336

www.elsevier.com/locate/joes

Original Article

Influence of temperature and salinity on hydrodynamic forces

A. Escobar*, V. Negro, J.S. López-Gutiérrez, M.D. Esteban

Technical University of Madrid, C/Profesor Aranguren S/N, 28040 Madrid, Spain

Received 26 June 2016; received in revised form 31 August 2016; accepted 21 September 2016
Available online 9 November 2016

Abstract

The purpose of this study is to introduce an innovative approach to offshore engineering so as to take variations in sea temperature and salinity into account in the calculation of hydrodynamic forces. With this in mind, a thorough critical analysis of the influence of sea temperature and salinity on hydrodynamic forces on piles like those used nowadays in offshore wind farms will be carried out. This influence on hydrodynamic forces occurs through a change in water density and viscosity due to temperature and salinity variation. Therefore, the aim here is to observe whether models currently used to estimate wave forces on piles are valid for different ranges of sea temperature and salinity apart from observing the limit when diffraction or nonlinear effects arise combining both effects with the magnitude of the pile diameter. Hence, specific software has been developed to simulate equations in fluid mechanics taking into account nonlinear and diffraction effects. This software enables wave produced forces on a cylinder supported on the sea bed to be calculated. The study includes observations on the calculation model's sensitivity as to a variation in the cylinder's diameter, on the one hand and, on the other, as to temperature and salinity variation. This software will enable an iterative calculation to be made for finding out the shape the pressure wave caused when a wave passes over will have for different pile diameters and water with different temperature and salinity.

Keywords: Sea temperature; Salinity; Hydrodynamic forces; Wave action; Offshore wind farms.

1. Introduction

Nowadays, most standards applied in the world in the field of offshore wind farm design, have the Morison formula as a central pillar of the calculation method for predicting hydrodynamic forces on a vertical circular cylinder, using Airy's theory to assess the field of speeds and accelerations of sea waves. On the other hand, for large diameter piles, the equation proposed by MacCamy & Fuchs is the basis for the calculation to take diffraction effects into account. This second equation also uses the linear theory to obtain the flow of speed and acceleration. In this research, special software has been developed to take all the different wave theories into account: Stokes, Cnoidal and Stream Function; to suitably characterize the field of fluid speed and accelerations whatever may be the height, period and depth of sea waves. In addition, this software allows the nonlinear and diffraction effects to be calculated for all cases: separate flow, inertial and diffraction range; and takes into account the wave-structure interaction.

The limit between the uses of each of the theories is an important issue which must be defined taking into account the temperature and salinity effect, not only the ratio between wave-length, pile diameter and the Keulegan–Carpenter number. According to available measures, extreme data regarding sea temperatures may be found in the Arctic and Southern Ocean, with sea temperatures of 1 °C; and in the Persian Gulf or Gulf of Mexico, with temperatures reaching 35 °C. Regarding sea salinity, the variation is less profound except near the coastal region. River run-off introduces enough fresh water in circulation near the coast producing variable horizontal as well as vertical salinity. In the open sea, values range from 3.4 to 3.7% and reach values of 35% in some bodies of water, such as the Red Sea.

In this research, the scope of works encompasses, in first place, the assessment of the range of use of each of the theories taking into account variations in salinity and sea

* Corresponding author.
E-mail address: adrian.escobar.pastor@alumnos.upm.es (A. Escobar).

http://dx.doi.org/10.1016/j.joes.2016.09.004

temperature. Secondly, a sensibility analysis is undertaken in order to assess whether the influence of temperature and salinity is greater for large or small pile diameters. Finally, an estimation of the percentages of diffraction and nonlinear effects caused by changes in salinity and temperature is included.

2. State of the art

Wind energy has begun to play an increasingly relevant role in society over the last few decades. As the development of renewable energies increased, the main concern of researchers has been to find new sources for obtaining energy and new processes enabling cleaner, less expensive and, therefore, more efficient energy to be created. With this in mind, the use of offshore wind farms has been one of the major achievements of modern science for achieving this aim as suggested by Esteban et al. [1]. The main difficulty these structures display from the construction standpoint lies in the correct estimation of hydrodynamic loads the structure will have to withstand. It could be said that calculating hydrodynamic forces in offshore structures is one of the major, key issues for design engineers participating in maritime engineering as suggested by Negro et al. [2]. In addition, they will be very important for the study of the influence of each of the forces on a possible scouring at the pile's base as suggested by Matutano et al. [3].

Calculating hydrodynamic forces is a very difficult task since environmental conditioning factors are highly complex and there are interaction phenomena between structure and incident waves. Nevertheless, even though wave action is stochastic in nature, studying wave action as if it behaved in a regular fashion and estimating the hydrodynamic forces it will generate on the structure and its resulting movements are of the utmost interest to the engineer. This method is known as the approach from the design wave. This type of analysis is completely determinist and rests on three fundamental variables, the wave height, its period and the depth. There is another approach which, by using the probabilistic theory, works with the wave energy's spectrum. Statistic design parameters, extreme forces and major dynamic responses may be predicted by using this approach.

Different calculation methods are used in predicting hydrodynamic forces and resulting responses, depending on the type and size of a structure's members in the high seas in comparison with the wave length [4–7].

Existing methods for finding hydrodynamic forces in offshore structures are mainly based on the following techniques: the use of the Morison equation or techniques using the potential of speeds for sources and sumps in two-dimensional or three-dimensional flow. The three-dimensional method is generally used from amongst these methods for structures comprising large structural elements. If a structure is made up of small elements, the Morison equation or the two-dimensional method of source-sump distribution will be required.

Morison et al. [8] suggested that the two flow regimes generated by inertia forces and drag forces may be superimposed to obtain the total load varying in time per unit of length of a cylinder immobile in a plane flow field with an arbitrary free flow speed. The wave force on circular piles, within the diffraction range, was first calculated by MacCamy and Fuchs [9], who proposed that there was an exact mathematical solution presented by wave action according to the linear wave theory. Chakrabarti [10] obtained the hydrodynamic forces caused by nonlinear waves on a vertical cylinder, including the use of the diffraction theory by means of a compact equation and then compared the equation proposed with experimental results. Chakrabarti et al. [11] proposed a general equation for the wave force equation applicable to a randomly oriented submerged or semi-submerged cylinder. Then expressions were also proposed for wave pressures and forces on several different sized vertical cylinders with different distances between them. Hydrodynamic forces due to the interaction of the different linear waves propagating with arbitrary directions were found. Lighthill [12] made a methodological analysis describing the basic physical phenomena together with the applicable methods used for estimating hydrodynamic forces. His main contribution to the calculation of wave force by using the Morison equation lies in the proposal of a second order correction thereto. Turbulent forces induced (separate flow) in wave action subjected cylinders and some methods for predicting such forces are discussed by Graham [13].

Wave forces acting on a cylinder emerging in a regular wave field were measured and compared with those of the calculations based on the Morison equation [14]. Cook and Simiu [15] also worked on hydrodynamic forces on vertical cylinders applying Lighthill's correction with the aim of including nonlinear effects in the calculation. The 17th ITFC Ocean Engineering Committee undertook to compare the methods in order to calculate the movement of a semi-submergible body. They concluded with a summary of the final project results in which 34 computer programs from 28 different organizations were later described by Takagi et al. [16].

Faltinsen [17] made a detailed analysis of wave induced linear movements and second order loads as well as nonlinear problems and viscous loads. This study concluded that the Morison equation and methods based on the theory of potential are favorably similar to each other and to field or laboratory made experimental measurements.

As computing power increased by the development of hardware and software engineering, new, more sophisticated methods have been introduced in recent years to calculate the wave–structure interaction problem. Koutandos [18] presented a numerical study on wave interaction with rigid vertical barriers and computed the velocities and turbulence kinetic energy in the vicinity of the structure. Isaacson et al. [19] and Zhu [20] investigated wave interaction with a row of piles using the full wave theory. Zheng and Zhang [21] present an analytical model to predict the three-dimensional wave diffraction of a floating cylinder located in front of a vertical wall at a finite water depth. Feng et al. [22], provide a solution for a two-dimensional nonlinear wave–structure interaction problem by a desingularized integral method in combination with

a mixed Euler–Lagrange method. Cao and Beck [23], present the derivations of different forms of integral desingularized boundary equations and discuss their fundamental aspects and advantages for studying water wave dynamics and body motion dynamics. Meng and Zhang [24] develop a third-order KdV solution for internal solitary waves by means of a new method based on weakly nonlinear assumptions in a rigid-lid two-layer system. Das [25] provides the solution to wave scattering by a horizontal circular cylinder in a three-layer fluid.

According to the current state of the art in this field, this research can be seen to represents the first investigation focused on the influence of temperature and salinity on hydrodynamic forces.

3. Method

The different forces acting must be broken down in order to study the wave regime affecting a fixed cylindrical body in a water domain. To do this, the forces waves exert on such a body may be classed into:

a. Drag forces (also called the viscous type).
  a.1 "Form drag" $\bar{F}_p$ associated with normal tensions.
  a.2 "Friction drag" $\bar{F}_f$ associated with surface friction.
b. Forces of inertia.

According to the undulatory theory, these forces originate from the speed potential, ϕ:

$$\varphi = \varphi_I + \varphi_D \tag{1}$$

ϕ_I Incident waves.
ϕ_D Wave diffraction.

When the structure's diameter is much smaller than the wave length, $D << L$, incident waves are not significantly modified by the presence of the body (where D is the cylinder's diameter and L the wave length); the diffraction component, φ_D can therefore be ignored. The force due to continuous current flow acting on a cylinder is:

$$F_D = \frac{1}{2} \cdot \rho \cdot C_D \cdot D \cdot u \cdot |u| \tag{2}$$

where, F_D is the force per unit of length of the cylinder, ρ the fluid's density and C_D the coefficient of drag. The speed squared is written in the form $u \bullet |u|$ to ensure that the direction of the drag force is the same as the speed's flow. However, wave action is an oscillatory current and, in this case, there will be two additional terms contributing to the whole of the force.

$$F = \frac{1}{2} \cdot \rho \cdot C_D \cdot D \cdot u \cdot |u| + m' \cdot a + \rho \cdot V \cdot a \tag{3}$$

where $m'{\cdot}a$, is called the "force of the additional mass mobilized" (hydrodynamic-mass force), m' is the additional mass mobilized or hydrodynamic mass, $\rho \cdot V \cdot a$, is called the "Froude–Krylov force", and V is the cylinder's volume which, if we take a unit of length of the cylinder, is reduced to A, the cross section area. The additional mass mobilized is defined as the mass of fluid around the body which is accelerated with the body's movement due to the action of pressure.

There are two effects when the body remains immobile and the water moves with an acceleration a. First, the water surrounding the body will accelerate as described. The force of the hydrodynamic mass will therefore be present. The second effect will be the fluid's accelerated movement in the external region of the flow generating a pressure gradient according to:

$$\frac{\partial p}{\partial x} = -\rho \cdot \frac{du}{dt} \tag{4}$$

where u is the speed of the fluid far from the cylinder. This pressure gradient will produce an additional force on the cylinder, which we call the Froude–Krylov force. This force may be calculated by the following integration:

$$F_p = -\int_s p \cdot dS \tag{5}$$

where S, is the body's surface area. From the Ostrogadski–Gauss theorem, we have:

$$F_p = -\int_V \frac{\partial p}{\partial x} \cdot dV = \int_V \rho \cdot \frac{du}{dt} \cdot dV \tag{6}$$

If we bear in mind that the pressure gradient is constant, the force per unit of length, F_p, for a cylinder with a cross section area, A, is:

$$F_p = \rho \cdot A \cdot a \tag{7}$$

The total force, F, is given by the foregoing expressions bearing in mind the force of the hydrodynamic mass and the Froude–Krylov force:

$$F = \frac{1}{2} \cdot \rho \cdot C_D \cdot D \cdot u \cdot |u| + \rho \cdot C_m \cdot A \cdot a + \rho \cdot A \cdot a \tag{8}$$

Knowing that $C_M = C_m + 1$, the classic expression of Morison, Johnson, Schaaf & O'Brien is given by:

$$F = \frac{1}{2} \cdot \rho \cdot C_D \cdot u \cdot |u| + \rho \cdot C_M \cdot A \cdot a = \rho \cdot \frac{D}{2} \cdot C_D \cdot u \cdot |u| + \rho \cdot \frac{\pi \cdot D^2}{4} \cdot C_M \cdot a \tag{9}$$

where:

- D: pile diameter
- A: cross section area of the vertical cylinder
- C_M: coefficient of inertia due to the hydrodynamic mass
- C_D: drag coefficient.

Morison proposed that inertial forces should be superimposed on drag forces in order to calculate the hydrodynamic forces on the cylinder.

The coefficients C_M and C_D are found empirically and basically depend on the Reynolds number, R_E, the Keulegan-Carpenter number and the cylinder's surface roughness. A multitude of studies has been carried out by many authors in

order to establish C_M. The criterion proposed by the Shore Protection Manual for establishing the coefficient C_M will be used as from the different studies shown in the foregoing table. In addition, the criterion used by the Shore Protection Manual is also taken into account to find the coefficient C_D, as from the studies of Achenbach (1968).

$$C_M = 2.0 \quad \text{when } R_E < 2.5 \cdot 10^5 \tag{10}$$

$$C_M = 2.5 - R_E/5 \cdot 10^5 \quad \text{when } 2.5 \cdot 10^5 < R_E < 5 \cdot 10^5 \tag{11}$$

$$C_M = 1.5 \quad \text{when } R_E > 5 \cdot 10^5 \tag{12}$$

$$C_D = 1.2 \quad \text{when } R_E < 1 \cdot 10^5 \tag{13}$$

$$C_D = 1.2 - \left(1.2 - 0.7/3 \cdot 10^5\right) \cdot \left(R_E - 10^5\right) \quad \text{when } 1 \cdot 10^5 < R_E < 4 \cdot 10^5 \tag{14}$$

$$C_D = 0.7 \quad \text{when } R_E > 4 \cdot 10^5. \tag{15}$$

The Reynolds number is calculated as:

$$R_E = \frac{u \cdot D}{\nu} \tag{16}$$

Variations in the sea temperature and salinity will change viscosity, ν, and water density, ρ. Hence, they will influence the total force generated because of the variation in density and, therefore will also influence the percentage of each type of force because they influence the Reynolds number, so affecting the C_M and C_D coefficients. Water viscosity and density are obtained in the calculation by relations established by Chakrabarti [26] from values of water temperature and salinity.

On the other hand, the diffraction equations are included in the problem statement, by taking into account the cylindrical coordinates:

$$\Delta\varphi_I = \frac{\partial^2\varphi_I}{\partial r^2} + \frac{1}{r}\frac{\partial\varphi_I}{\partial r} + \frac{1}{r^2}\frac{\partial^2\varphi_I}{\partial\theta^2} + \frac{\partial^2\varphi_I}{\partial z^2} = 0, \quad \text{in } \Omega \tag{17}$$

$$\frac{\partial\varphi_D}{\partial r} = -\frac{\partial\varphi_I}{\partial r}, \quad \text{when } r = b \tag{18}$$

$$\frac{\partial\varphi_I}{\partial z} = 0, \quad \text{when } z = 0 \tag{19}$$

$$\frac{\partial^2\varphi_I}{\partial t^2} + g\frac{\partial\varphi_I}{\partial z} = 0, \quad \text{when } z = d. \tag{20}$$

If the Sommerfeld condition is shown as a complex expression:

$$\lim_{r\to\infty}\sqrt{r}\left(\frac{\partial\varphi_D}{\partial r} - ik\varphi_D\right) = 0 \tag{21}$$

With $D/2 = b$, the velocity potential can be obtained in terms of the first type of the Bessel function J_n and Hankel functions of the first type H_n:

$$\varphi_I = Re\left[-\frac{gH}{2\omega}\frac{\cosh kz}{\cosh kd}\sum_{n=0}^{\infty}\varepsilon_n i^n J_n(kr)\cos n\theta e^{-i\omega t}\right] \tag{22}$$

$$\varphi_D = Re\left[+\frac{gH}{2\omega}\frac{\cosh kz}{\cosh kd}\sum_{n=0}^{\infty}\varepsilon_n i^n \frac{J_n'(kb)}{H_n'(kb)} H_n(kr)\cos n\theta e^{-i\omega t}\right] \tag{23}$$

The velocity potential can be expressed as:

$$\varphi = \varphi_I + \varphi_D = Re\left[-\frac{gH}{2\omega}\frac{\cosh kz}{\cosh kd} \sum_{n=0}^{\infty}\varepsilon_n i^n\left[J_n(kr) - \frac{J_n'(kb)}{H_n'(kb)}H_n(kr)\right]\cos n\theta e^{-i\omega t}\right] \tag{24}$$

From the above expression, the Froude–Krylov force exerted by the waves on the cylinder is obtained by the following expression:

$$F = \frac{2\pi}{k}\ \rho g\frac{HD}{4}\tanh kdRe \left[-\left(J_1(kb) - \frac{J_1'(kb)}{H_1'(kb)}H_1(kb)\right)e^{-i\omega t}\right] \tag{25}$$

4. Calculation model

The methodology developed to suitably solve the problem must follow the following scheme (Figs. 1 and 2).

In the first place, the software takes the environmental conditions: wave period (T) and height (H), and sea depth (d); as first order variables which define the wave mechanics to handle in the calculation as the basis of the whole assessment. Moreover, this section takes the influence of temperature (Ta) and salinity (S) on the water density (ρ) into account as a second order effect. In this step of the calculation, the range of the problem (deep water, intermediate depth and shallow water) has to be identified and the equations which define the water wave motion solved (Euler equations of motion and continuity equation).

$$\frac{\partial u_i}{\partial t} + u_j\frac{\partial u_i}{\partial x_j} + w\frac{\partial u_i}{\partial z} = -\frac{1}{\rho}\frac{\partial p}{\partial x_i} \tag{26}$$

$$\frac{\partial w}{\partial t} + u_j\frac{\partial w}{\partial x_j} + w\frac{\partial w}{\partial z} = -g - \frac{1}{\rho}\frac{\partial p}{\partial z} \tag{27}$$

$$\frac{\partial u_j}{\partial x_j} + \frac{\partial w}{\partial z} = 0 \tag{28}$$

To solve the system, the software will use the pertinent wave theory (such as Airy, Stokes, Cnoidal or Stream Function) according to the classification of Le Méhauté shown in Fig. 3.

In second place, the software assesses the hydrodynamic loads on the basis of flow speeds (v) and accelerations (a)

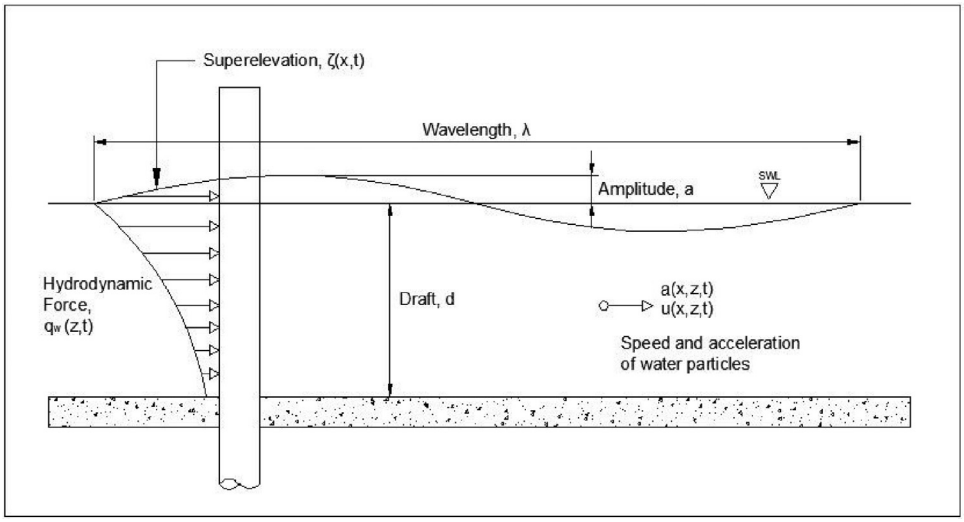

Fig. 1. Diagram of wave action on a pile.

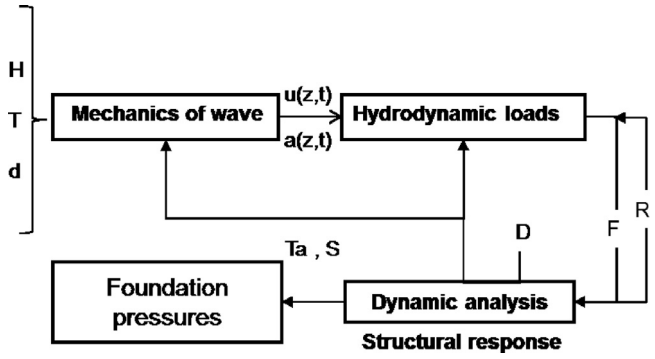

Fig. 2. Calculation scheme.

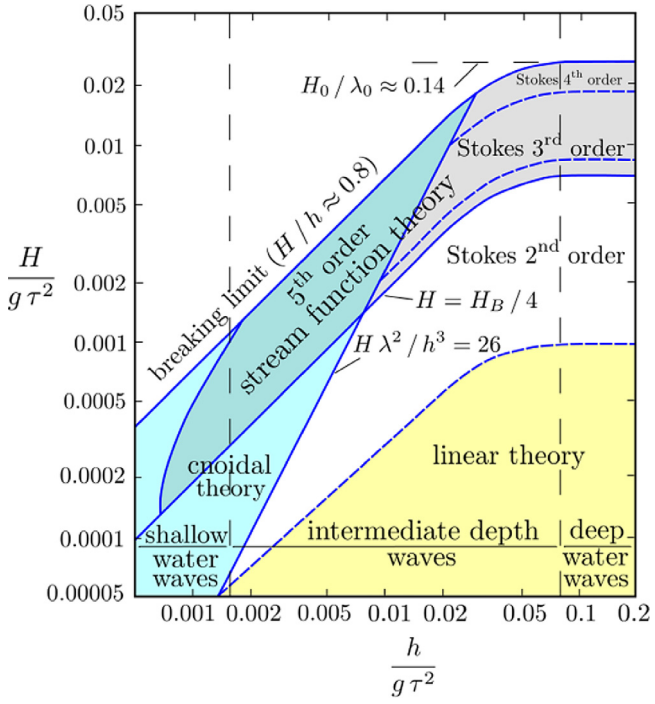

Fig. 3. Wave theories classification by Le Méhauté.

obtained in the last step. This problem has the diameter of the pile (D) as a first order variable, In conjunction with wave mechanics the pile diameter defines the range (separate flow, inertial or diffraction) in which the problem must be solved. Sea temperature and salinity are included again because they play a key role in this part because of their influence on water viscosity and hence on drag forces. The assessment of hydrodynamic loads will provide the solution for one of the ranges: separate flow, inertial and diffraction; taking into account nonlinear effects, as appropriate. The range is identified by three parameters: Keulegan–Carpenter number, ratio H/L and ratio D/L:

The separate flow range is solved by means of Morison's equation. Furthermore, nonlinear effects of the second order terms of the wave motion will be introduced analytically in accordance with the corrections provided by Lighthill (as F_3, F_4 and F_5) for the cases in which the problem is located in the separate nonlinear flow range:

$$F(z,t) = F_1 + F_2 + F_3 + F_4 + F_5 \tag{29}$$

$$F_1 = -\rho \int_{\partial\Omega} \frac{\partial \varphi_1}{\partial t} n \, ds = \frac{1}{4} C_M \rho \pi D^2 \cdot a(z,t);$$

$$F_2 = \frac{1}{2} C_D \rho D \cdot u(z,t) \cdot |u(z,t)| \tag{30}$$

$$F_3 = -\rho \int_{z=d} w(\nabla\varphi_1)^2 ds; \quad F_4 = \frac{1}{2}\rho \int_S (\nabla\varphi_1)^2 \cos\theta ds;$$

$$F_5 = \frac{\rho}{2g} \oint_C \left(\frac{\partial \varphi_l}{\partial t}\right)^2 \cos\theta dl \tag{31}$$

The inertial range uses the same equation, shown above for the separate flow range, but removes the term F_2 corresponding to drag force (Table.1). On the other hand, when

Table 1
Range classification.

	KC < 4 $H/L < 0.5\,H/L_{max}$	KC < 4 $H/L > 0.5\,H/L_{max}$	KC > 4 $H/L < 0.5\,H/L_{max}$	KC > 4 $H/L > 0.5\,H/L_{max}$
$D/L < 0,\ 2$	Linear inertial range	Nonlinear inertial range	Linear separate flow range	Nonlinear separate flow range
$D/L > 0,\ 2$	Linear diffraction range	Nonlinear diffraction range	-	-

the assumption that the kinematics of the undisturbed flow in the region near the structure do not change in the incident wave direction is not fulfilled, the diffraction theory has to be used. The theory provided by MacCamy and Fuchs is used as a basis (F_1) but adding additional terms to include non-linear effects in the calculation (F_2), using the perturbation parameter (ε).

$$F(z,t) = \varepsilon F_1 + \varepsilon^2 F_2 \tag{32}$$

$$F_1(z,t) = -D\rho \int_0^{2\pi} \left(\frac{\partial \varphi^{(1)}}{\partial t}\right)_{r=D} \cos(\pi - \theta)\ d\theta \tag{33}$$

$$F_2(z,t) = -D\rho \int_0^{2\pi} \left[\int_0^{\eta^{(1)}} \left(\frac{\partial \varphi^{(1)}}{\partial t} + gz\right) dz + \frac{\partial \varphi^{(2)}}{\partial t} + \frac{1}{2}\left(\frac{\partial \varphi^{(1)}}{\partial z}\right)^2 + \frac{1}{2D^2}\left(\frac{\partial \varphi^{(1)}}{\partial \theta}\right)^2 \right]_{r=D} \cos(\pi - \theta) d\theta \tag{34}$$

Finally, the third step takes the sea wave loads obtained and assesses their effect on the foundation and on the movements of the structure along the vertical axis. Finally, the structure movements and the loads generated by them feed the second section again and allow the calculation to be iteratively made again until a final solution is achieved. The structural response analysis is performed in the field of elastic deformation. The vertical circular cylinder is assumed to be a cantilever beam fixed in the sea bed. The calculations must apply a dynamic assessment in the frequency domain, which takes the inertial effects into account. The differential equation which defines the behavior of the cantilever beam is:

$$EI\frac{\partial^4 x(z,t)}{\partial z^4} + m\frac{\partial^2 x(z,t)}{\partial t^2} = 0 \tag{35}$$

where, EI is the beam stiffness and m the beam mass. The above equation is best solved by separating variables. If it is assumed that the displacement can be separated into two parts, one depends on position and the other on time, which are both independent of each other, so that the equation can now be written as two differential equations:

$$x(z,t) = Z \cdot T;\ \ \frac{\partial^4 Z}{\partial z^4} - k_n^4 Z = 0;\ \ \frac{\partial^2 T}{\partial t^2} + \omega_n^2 T = 0 \tag{36}$$

where ω_n represents the natural frequencies of the beam, and k_n is as follows:

$$k_n^4 = \frac{w_n^2 m}{EI} \tag{37}$$

The solution of the system is given by:

$$x(z,t) = \sum_{m=1}^{\infty} Z_n(z)[A_n \cos(\omega_n t) + B_n \sin(\omega_n t)]. \tag{38}$$

A_n depends on the initial position at time $t=0$, B_n depends on the initial velocity, and both of them must be determined with the boundary conditions.

$$A_n = \frac{\int_0^d x_0(z) Z_n(z) dz}{\int_0^d Z_n^2(z) dz};\ \ B_n = \frac{1}{\omega_n}\frac{\int_0^d v_0(z) Z_n(z) dz}{\int_0^d Z_n^2(z) dz} \tag{39}$$

Then, the load $F\ (z,\ t)$ is introduced into the differential equations as a boundary condition to obtain $A_{n,i+1}$ and $B_{n,i+1}$, for the next time step. For each time step, the speed and acceleration of the following time step can be obtained by the following equation

$$A_{n,i+1} = \frac{1}{\omega_n^2 \rho_{est} A}\frac{\int_0^d \Delta F(z) Z_n(z) dz}{\int_0^d Z_n^2(z) dz};$$
$$B_{n,i+1} = \frac{1}{\omega_n}\frac{\int_0^d v_i(z) Z_n(z) dz}{\int_0^d Z_n^2(z) dz} \tag{40}$$

$$\Delta F(z) = F(z,\ t = t_{i+1}) - R(z,\ t = t_i) \tag{41}$$

where:

- $F(z,\ t{=}t_{i+1})$: hydrodynamic forces in $ti+1$.
- $R(z,\ t{=}t_i)$: structural response in ti.
- ρ_{est}: density of structural element.
- A: area of structural element.

The function Z_n and the modes of vibration k_n are determined by the following equations:

$$Z_n(z) = \frac{1}{2}\left\{[\cos(k_n z) - \cosh(k_n z)] + \left[\frac{-\cos(k_n d) - \cosh(k_n d)}{\sin(k_n d) - \sinh(k_n d)}\right][\sin(k_n z) - \sinh(k_n z)]\right\} \tag{42}$$

$$\cos(k_n d)\cosh(k_n d) = -1 \tag{43}$$

Using this kind of analysis, the speed and acceleration of each point of the structure can be obtained as a response of the hydrodynamic loads to each time step. These speeds and accelerations can be subtracted from the initial $v\ (z,\ t)$ and $a\ (z,\ t)$, and the process repeated until its convergence for each fraction of time. The final result is a full record of the movements of the structure along the whole length originated by sea waves. Finally, the bending moment on the foundation can be easily obtained from these structural movements.

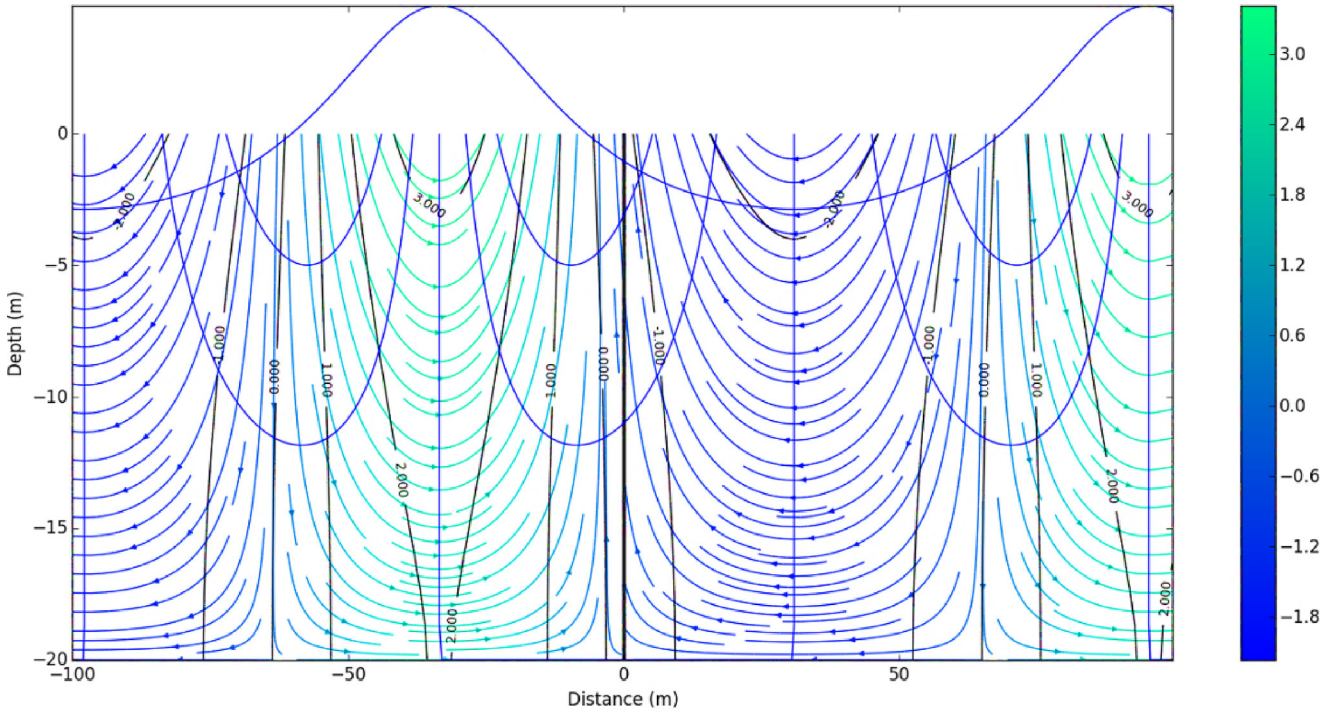

Fig. 4. Field of sea wave speeds.

5. Results

Seven cases were defined for undertaking the study and only the cylinder's diameter, the sea's temperature and salinity varies in them whilst waves are taken to be regular. Case 1 will address a diameter of 0.5 m, case 2, a diameter of 2 m, case 3, a diameter of 4 m, case 4, a diameter of 8 m, case 5, a diameter of 16 m, case 6, a diameter of 20 m, and case 7, a diameter of 26 m. All these diameters have been chosen according to the standard types of offshore wind farms, from the first models with 0.5 m to those used nowadays as in: Scarweather Sands (United Kingdom) with 2.2 m, Princess Amalia (Netherlands) with 4.0 m and, Nysted (Denmark) or Thornton Bank (Belgium) with diameters from 6.5 m up to 17 m; the values of 20 and 26 m have been included to take into account the future piles due to the fact that, maybe in the next few years, pile diameters will keep increasing to support a heavier and more powerful wind turbine in keeping with the requirements of the offshore industry (Figs. 4–Fig. 12).

The flow of speeds and accelerations has been calculated for them all, taking into account the possible diffraction and nonlinear effects for two sub-cases. Case A will have a sea temperature of 1 °C and 0% salinity, and case B will be performed with a sea temperature of 22 °C and salinity of 35%. The common details for regular sea waves to be entered in all the study cases have been obtained from those used in the design of Princess Amalia (Netherlands):

- Wave height: 7.5 m.
- Depth: 20.0 m.
- Period: 10 s.

According to this data, the wave theory will be Stokes' 3rd order in transition depth.

$$\delta_1 = \frac{H}{gT^2} = 0.00764 \quad \delta_2 = \frac{h}{gT^2} = 0.02038 \tag{44}$$

$$\frac{d}{L} = \frac{20}{128.7} \rightarrow 0.4 < 0.155 < 0.5 \rightarrow Transition\ depth \tag{45}$$

The field of accelerations and speeds for the case of height 7.5 m, depth 20.0 m and period 10 s, calculated by the software developed is shown below:

According to those values, the force for the case of a sea temperature of 1 °C and 0% salinity and for the case of a sea temperature of 22 °C and salinity of 35% will calculated, as, respectively, F_1 and F_2. The following figures show the percentages of $|F_{i1}\text{-}F_{i2}|/F_{t2}$, where F_{i1} and F_{i2} are the different components of the total force: inertial forces, drag forces, diffraction forces and nonlinear forces; and F_{t2}, the total forces obtained in the second case. All this is for the different time steps throughout the whole time period of 10 s, for the sea surface and for the bottom.

According to the values shown above, the maximum variations for all cases are summarized below:

The variation suffered by the drag forces can initially be seen to drastically reduce on the pile diameter increasing whilst the variation of inertial force is increasing enormously and becomes the predominant variation. The influence of temperature and salinity is shown to be clearly higher on the bottom than on the free surface for the cases with diameters: 0.5, 8.0, 16.0, 20.0 and 26.0. For those cases with diameter 2.0 and 4.0, there is almost the same influences on the bottom and the surface.

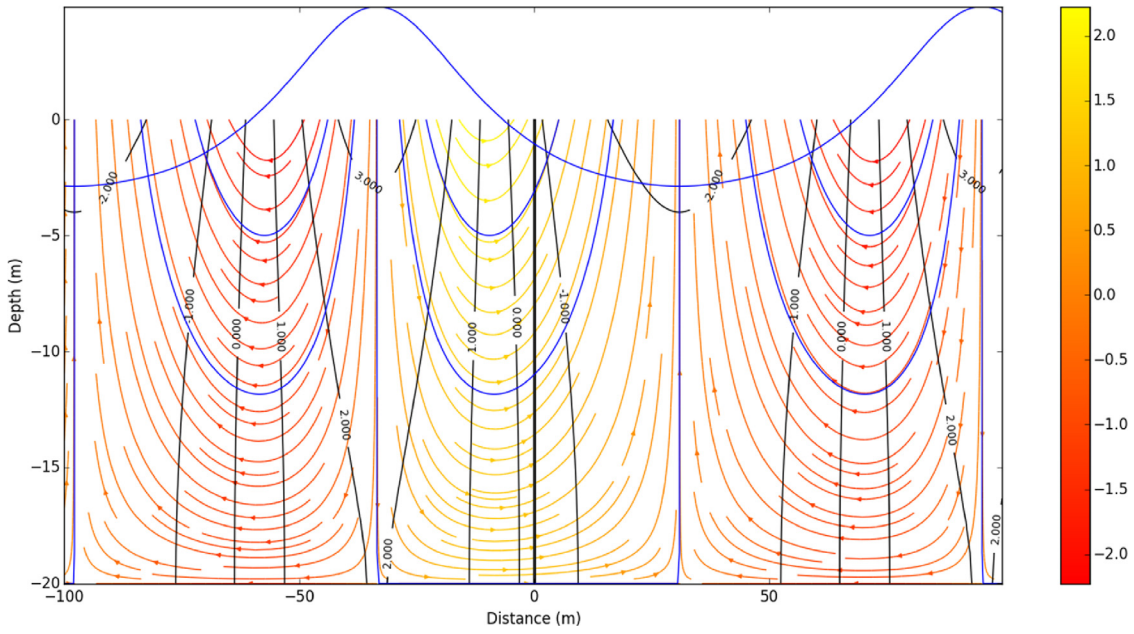

Fig. 5. Field of sea wave accelerations.

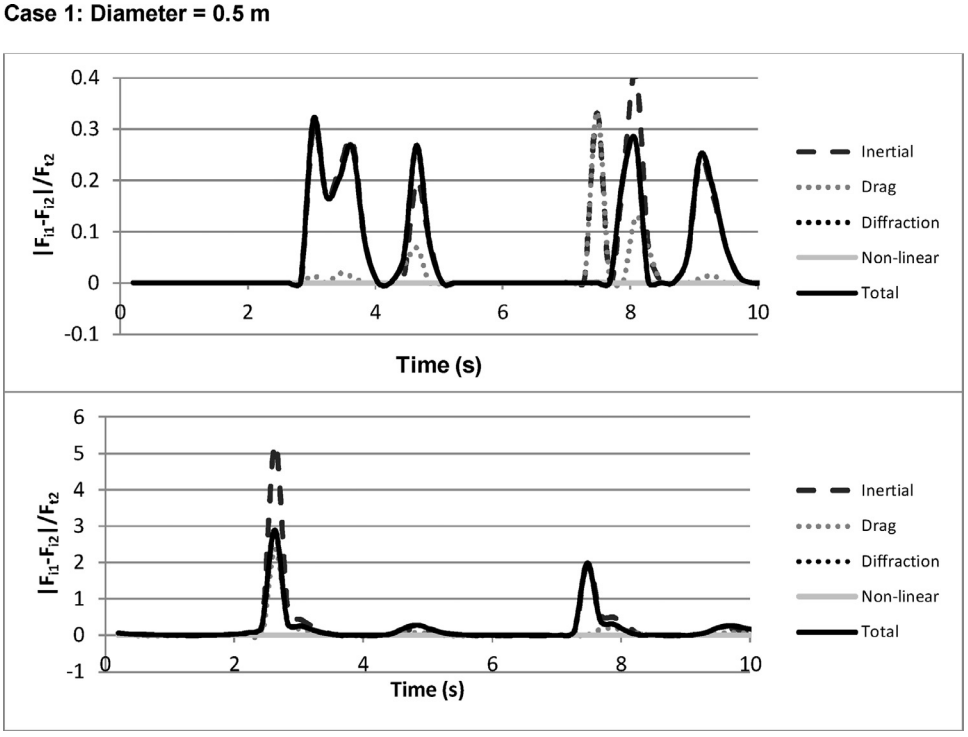

Fig. 6. Simulation with $D = 0.5$ m, on a free surface in the figure above, and at the sea bed in the figure below.

The reason for this is that the inertial force is discontinuous for the largest diameters. This manifests as a leap or step in the wave crest. This leap gradually disappears as the diameter increases and is caused by a change in the coefficients C_D and C_M. As explained earlier, these coefficients vary with the Reynolds number and as the dynamic viscosity and diameter remain constant during the calculation of one case, the leap is indicating that at that point, speed is varying enough for the Reynolds number to become less than 2.5×10^5, making C_M 2.0.

There is a different reason for the 0.5 m diameter as drag forces which generate a large variation if the load profile for changes in temperature and salinity are heavily influential.

The diameters of 2.0 m and 4.0 m are cases in the transition between the end of the range of separate flow and the beginning of the inertial range, so the effect generated by

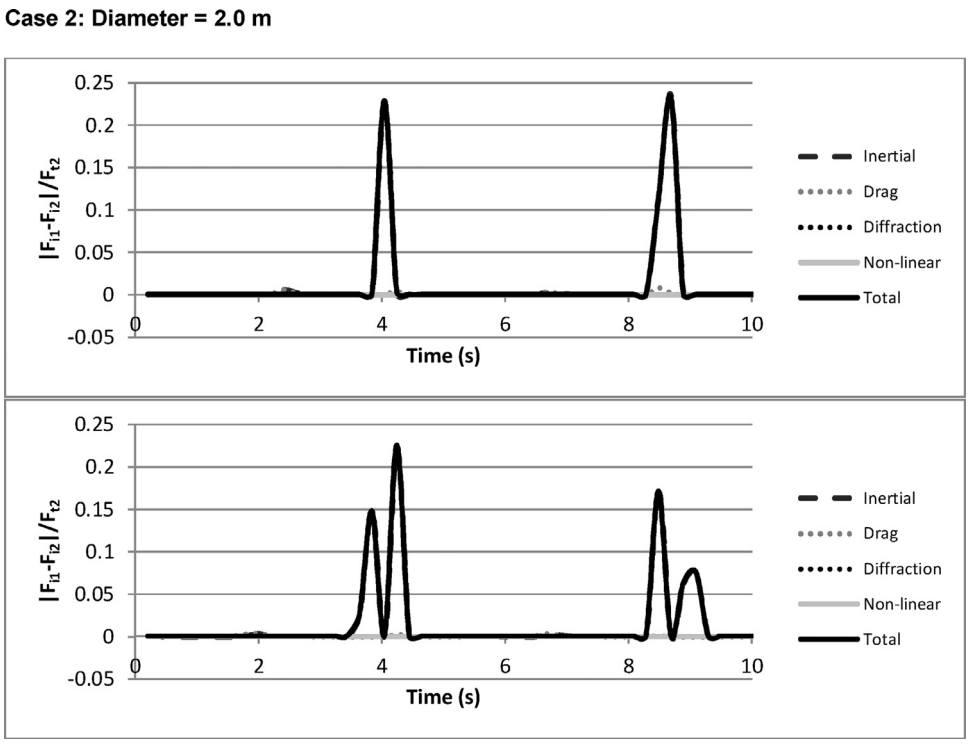

Fig. 7. Simulation with $D = 2.0$ m, on a free surface in the figure above, and at the sea bed in the figure below.

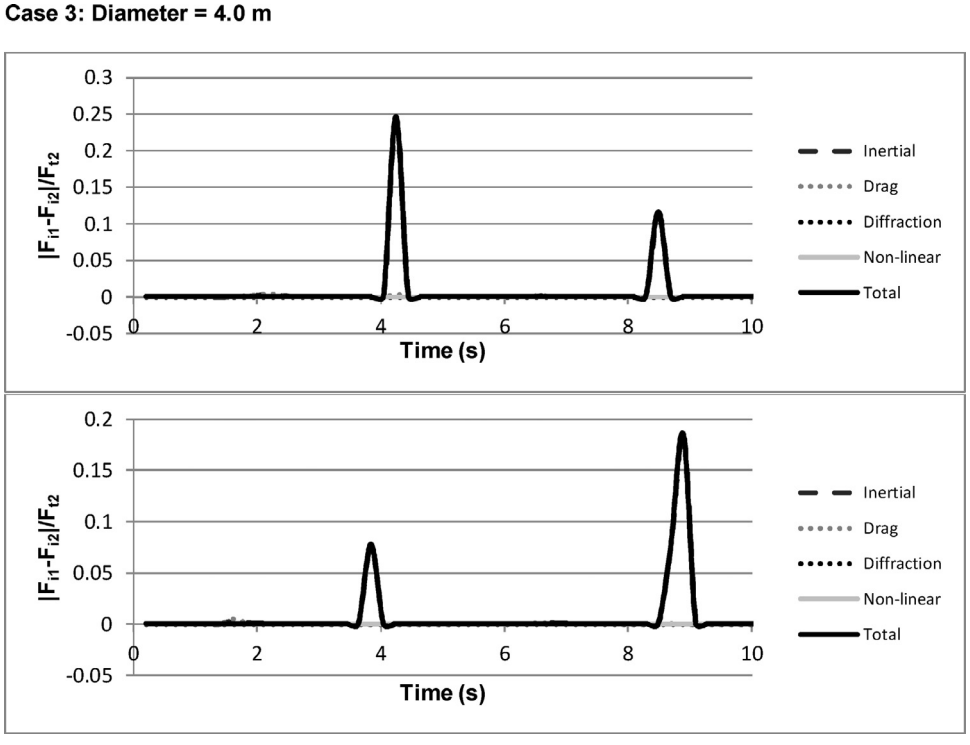

Fig. 8. Simulation with $D = 4.0$ m, on a free surface in the figure above, and at the sea bed in the figure below.

drag forces is disappearing but the effect of discontinuity in inertial forces influences the whole depth.

The higher the temperature values, the greater is the wave deformation observed. Discontinuities can also be observed in the case with a sea temperature of 22 °C and salinity of 35% showing a narrower width than those appearing in the case of a sea temperature of 1 °C and salinity of 0.0%, so the temperature increase could be assimilated to a virtual pile diameter increase in terms of the shape of the load profile of the wave. In addition, the width this discontinuity shows can

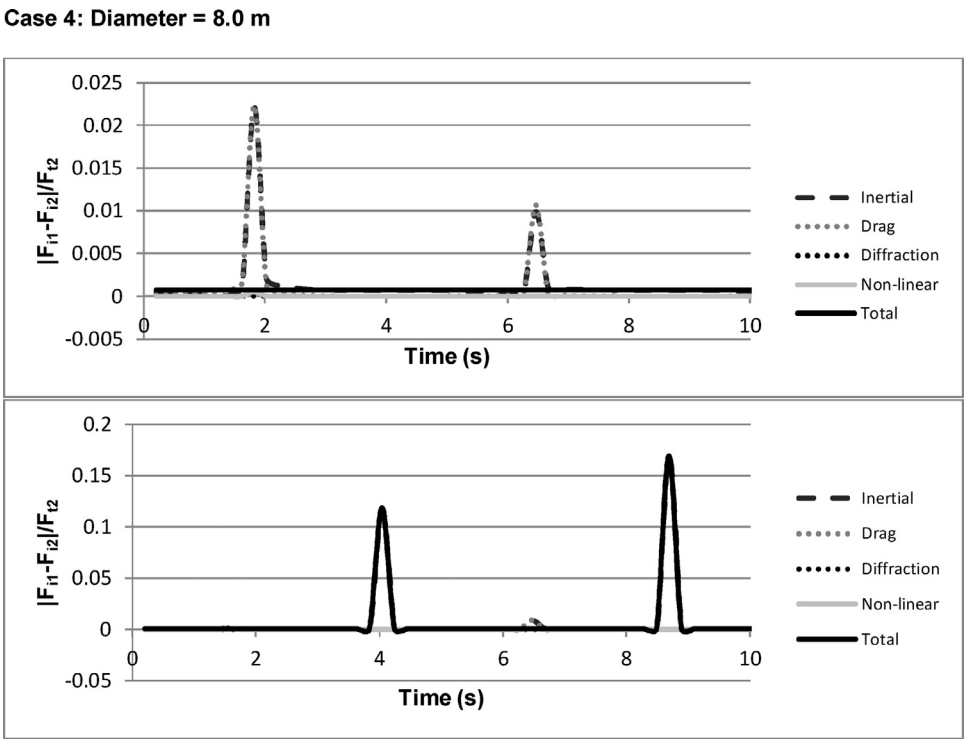

Fig. 9. Simulation with $D = 8.0$ m, on a free surface in the figure above, and at the sea bed in the figure below.

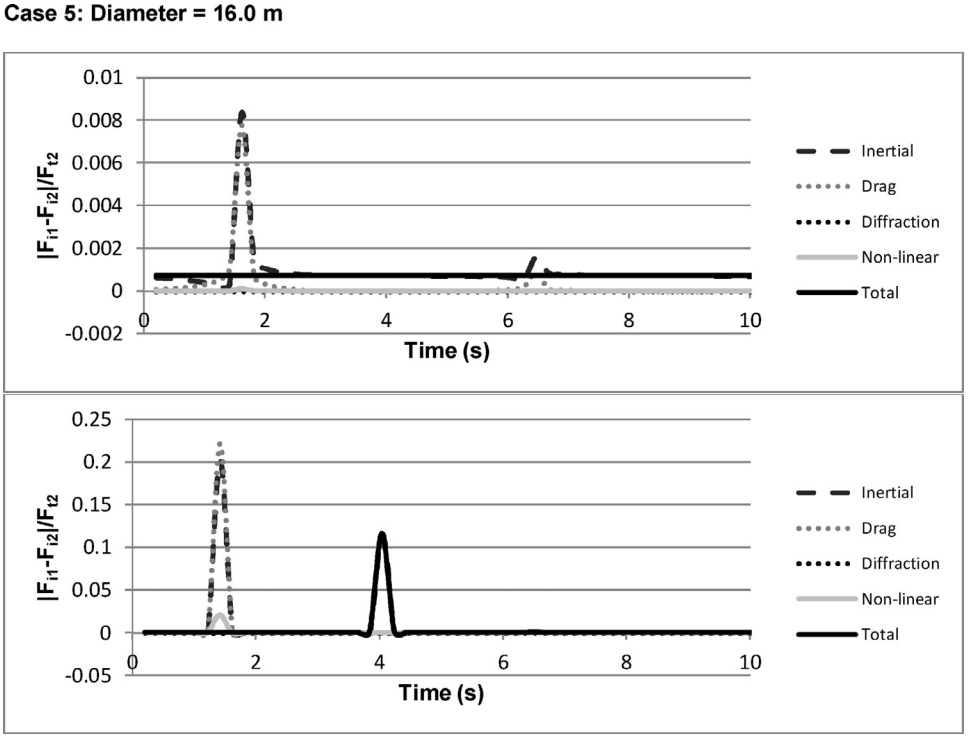

Fig. 10. Simulation with $D = 16.0$ m, on a free surface in the figure above, and at the sea bed in the figure below.

also be observed to be always narrower at the surface than at the sea bed.

All of the results shown above demonstrate the major differences generated in the load profile of sea waves after the temperature and salinity change. However, the maximum influence has to be demonstrated by using the ratio between the maximum total forces generated in both temperature cases for each diameter, in order to obtain the actual influence in terms

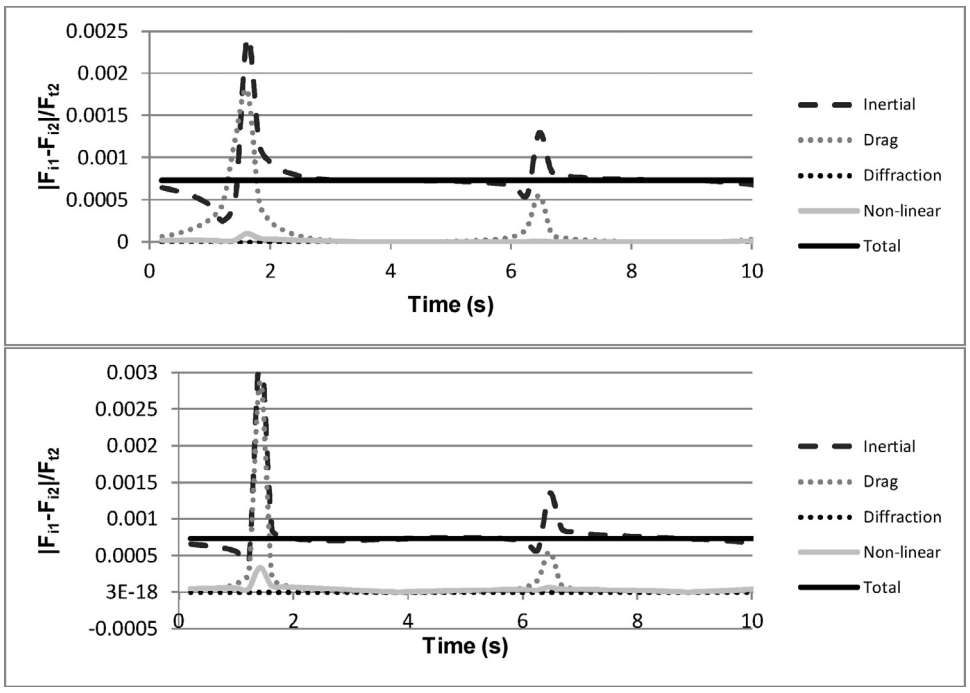

Fig. 11. Simulation with $D = 20.0$ m, on a free surface in the figure above, and at the sea bed in the figure below.

Case 7: Diameter = 26.0 m

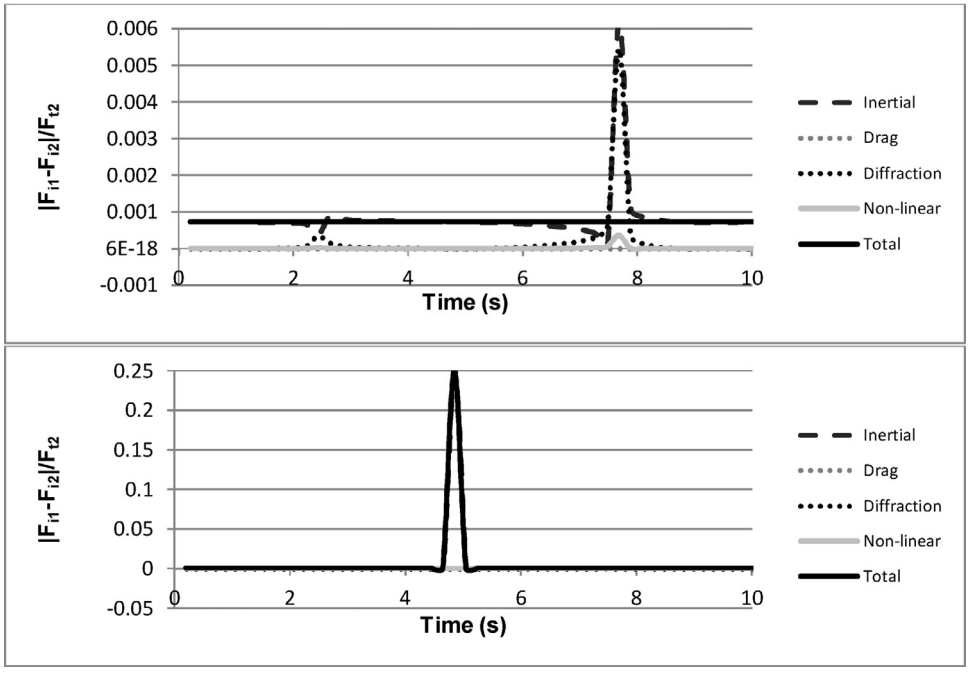

Fig. 12. Simulation with $D = 26.0$ m, on a free surface in the figure above, and at the sea bed in the figure below.

of maximum values.

$$\% = \frac{F_{22^\circ C,\ 35\%\ S} - F_{1^\circ C,\ 0\%\ S}}{F_{1^\circ C,\ 0\%\ S}} \tag{46}$$

Table 3 shows that the maximum value of the total force generated is higher for the case of 1 °C and salinity of 0.0% than the force generated in the case of 22 °C and salinity of 35%. But the higher the diameter values, the smaller are the influences of temperature and salinity. However, the variations observed in Table 3 for the total load are quite smaller than those shown in Table 2, so maximum variations are not necessarily related to maximum loads.

Table 2
Maximum variations shown for each type of force.

	Inertial F.		Drag F.		Diffraction F.		Nonlinear F.		Total	
Diameter	Surface	Bottom	Surface	Bottom	Surface	Bottom	Surface	Bottom	Surface	Bottom
$D=0.5$	40.80%	527.27%	33.44%	238.02%	0.00%	0.00%	0.19%	0.14%	31.95%	289.11%
$D=2$	23.47%	22.27%	0.83%	0.35%	0.00%	0.00%	0.02%	0.03%	23.22%	22.54%
$D=4$	24.30%	18.54%	0.44%	0.54%	0.00%	0.00%	0.01%	0.04%	24.65%	18.54%
$D=8$	2.22%	16.94%	2.24%	0.95%	0.00%	0.00%	0.05%	0.04%	0.07%	16.93%
$D=16$	0.84%	20.17%	0.78%	22.17%	0.00%	0.00%	0.01%	2.08%	0.07%	11.61%
$D=20$	0.24%	0.33%	0.18%	0.29%	0.00%	0.00%	0.01%	0.03%	0.07%	0.07%
$D=26$	0.62%	25.08%	0.00%	0.00%	0.55%	0.05%	0.04%	0.02%	0.07%	25.08%

Table 3
Influence on the maximum force generated.

	Total	
Diameter	Surface	Bottom
$D=0.5$	0.07%	–10.73%
$D=2$	–2.12%	–1.06%
$D=4$	–0.96%	–0.47%
$D=8$	–0.46%	–0.19%
$D=16$	–0.12%	–0.07%
$D=20$	–0.10%	–0.04%
=26	–0.09%	–0.01%

6. Conclusions and discussion

The intention throughout this study was to observe the influence of temperature and salinity on hydrodynamic forces. As observed, temperature and salinity act as a diameter amplifying component allowing the discontinuity or leap very clearly observed in inertia forces, to reduce in width. This width is the amount of time during which that discontinuity manifests. This effect is also observed when increasing the pile's diameter and therefore the increase in temperature and salinity is partly assimilated to the effect that an increase in diameter would have. However, viewed from the perspective of maximum loads generated, an increase in temperature has the opposite effect, giving maximum forces for the lower values of temperature and salinity.

It may be noted also that the maximum influence is exerted on elements with the smallest diameters and at the sea bed, so for large diameters, the influence has almost disappeared on the free surface.

Finally, it may be concluded that the influence of temperature and salinity acts over the whole load profile of the wave, but has minimum influence on maximum load values. Hence, neither parameter will have any influence on simplified models of calculation which do not take the dynamic behavior of the structure and the coupling between the sea waves and the structural elements into account. However, correct values of temperature and salinity will have to be observed in complex calculation models as developed for the current research which takes into account the whole load profile of the sea wave due to the variations of the load profile generating a variation in the induced vibrations over the structure. Therefore, these temperature and salinity variations will be able to generate load increments in the range of 15–30% in some cases, and need to be considered in modern calculation models.

References

[1] M.D. Esteban, J.J. Diez, J.S. López–Gutiérrez, V. Negro, Renew. Energy J. 36 (2011) 444–450, doi:10.1016/j.renene.2010.07.009.
[2] V. Negro, J.S. López-Gutiérrez, M.D. Esteban, C. Matutano, Renew. Energy J. 63 (2014) 125–132, doi:10.1016/j.rene.2013.08.041.
[3] C. Matutano, V. Negro, J.S. López–Gutiérrez, M.D. Esteban, Renew. Energy J. 57 (2013) 358–365 Beach Erosion Board, doi:10.1016/j.renene.2013.01.048.
[4] S.K. Chakrabarti, Nonlinear Methods in Offshore Engineering, Elsevier Science, New York, 1990.
[5] O.M. Faltinsen, Sea Loads on Ships and Offshore Structures, Cambridge University Press, Cambridge, 1990.
[6] J.P. Hooft, Advanced Dynamics of Marine Structures, John Wiley, New York, 1982.
[7] T. Sarpkaya, M. Isaacson, Mechanics of Wave Forces on Offshore Structures, Van Nostrand–Reinhold, New York, 1981.
[8] J.R. Morison, M.P. O'Brien, J.W. Johnson, S.A. Schaaf, Petrol. Trans. AIME 189 (1950) 149–154; A.M. Muir Wood, Coastal Hydraulics, Macmillan, New York, 1969.
[9] MacCamy, R.C. and Fuchs, R.A. 1954. Technical Memorandum No. 69, Beach Erosion Board, Corps of Engineers.
[10] S.K. Chakrabarti, J. Hydraul. Div., ASCE 98 (HYll) (1972) 1895–1909.
[11] S.K. Chakrabarti, W.A. Tam, A.L. Wolbert, in: Proceedings of the 7th Offshore Technology Conference, OTC 2190, Houston, Texas, 1975, pp. 433–447.
[12] J. Lighthill, in: Proceedings of the 2nd International Conference on the Behaviour of Offshore Structures, BOSS'79, London, 1979, pp. 1–40.
[13] J.M.R. Graham, Proceedings in Mechanics of Wave-induced Forces on Cylinders, Pitman, London, 1979, pp. 133–151.
[14] W. Koterayama, M. Nakamura, ASME Trans. J. Offshore Mech. Arctic Eng. 110 (1988) 315–319.
[15] G.R. Cook, E. Simiu, Ocean Eng. 16 (1989) 355–372.
[16] M. Takagi, S-I. Arai, S. Takezawa, K. Tanaka, N. Takarada, Ocean Eng. 12 (1985) 45–97.
[17] O.M. Faltinsen, Ann. Rev. Fluid Mech. 22 (1990) 35–56.
[18] E.V. Koutandos, WSEAS Trans. Fluid Mech. 4 (3) (2009) 85–96.
[19] M. Isaacson, S. Premasirl, G. Yang, J. Waterw. Port Coast. Ocean Eng. 124 (3) (1998) 118–126.
[20] D. Zhu, China Ocean Eng. 27 (3) (2013) 323–334.
[21] S. Zheng, Y. Zhang, Ocean Eng. 104 (2015) 329–343.
[22] A. Feng, Z. Chen, W. Price, Ocean Eng. 101 (2015) 131–141.
[23] Y. Cao, R.F. Beck, J. Ocean Eng. Sci. 1 (2016) 11–29.
[24] Q. Meng, C. Zhang, J. Ocean Eng. Sci. 1 (2016) 93–108.
[25] D. Das, J. Ocean Eng. Sci. 1 (2016) 135–148.
[26] S.K. Chakrabarti, Handbook of Offshore Engineering, Elsevier Science, New York, 2005.